



**Abstract**

The annular modes of the extratropical atmosphere have received much attention for quantifying variability of the jet streams and storm tracks, despite the fact that the midlatitude circulation itself does not vary uniformly with longitude. While tropical fluctuations in geopotential height have lower amplitude than in the extratropics, they exhibit stronger zonal coherence, or dynamical annularity. A simple index is developed to characterize zonal-mean anomalies of the tropical circulation. It reveals that anomalies in geopotential height and zonal wind migrate downward from the upper troposphere to the surface on a time scale of about 10 days. These features are distinguishable from known modes of tropical variability, the Madden–Julian Oscillation in particular. Evidence from reanalysis and idealized model experiments confirms that this downward migration is quite generic and driven by mechanically forced variations in the strength of the Hadley circulation on subseasonal time scales.

**Plain language summary:** Earth’s atmosphere has certain recurring patterns which are “annular,” spanning an entire latitude circle. Annular patterns have proven to be surprisingly useful for weather and climate prediction. However, in the tropics, annular patterns have not been studied. We show that annular variability in the tropics does exist, and it contains interesting features that may be useful for prediction. In particular, anomalies in the circulation migrate downward from the tropopause (about 16 km) to the surface over 10 days. These features are also apparent in a relatively simple climate model, which helps direct further research.

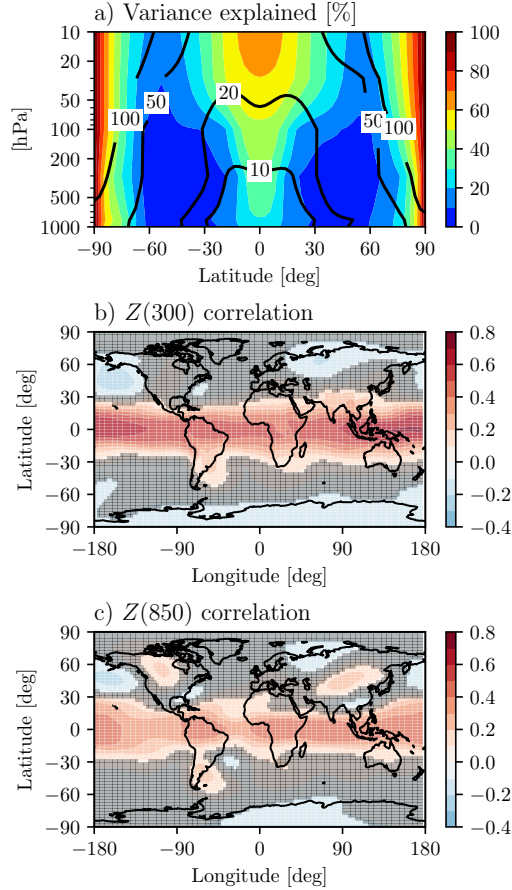
**1 Dynamical annularity of the atmospheric circulation**

The annular modes of the extratropical circulation have received much attention for their predictive utility and dynamical insight (see Kushner, 2010, for an extensive review). They characterize atmospheric variability in a remarkable variety of contexts, from unforced intraseasonal variability (e.g., Thompson & Wallace, 1998; Feldstein, 2000) to forced responses associated with global warming (Thompson et al., 2000) or stratospheric ozone loss and recovery (Thompson et al., 2002). The designation “annular” refers to their zonally uniform structure, which characterizes an exchange of mass and momentum between the polar cap and midlatitudes (Thompson & Wallace, 2000), although their dynamics fundamentally depends on zonally asymmetric eddies (Hartmann & Lo, 1998).

From the time of their discovery, however, there has been much debate on the extent to which an annular mode, or midlatitude variability more generally, is actually annular. Deser et al. (2000) and Ambaum et al. (2001) observed that while variability of geopotential height becomes zonally uniform over the polar cap in a trivial sense, as the latitude circle approaches the scale of the deformation radius, variations in the midlatitudes are not at all zonally uniform.

More recently, Gerber & Thompson (2017) attributed the zonal structure of the annular mode patterns to the “statistical annularity” of the midlatitude circulation. The annularity of the pattern reflects the fact that the statistics of geopotential height variability are fairly uniform across longitudes, as opposed to the fluctuations themselves. They observed, however, that geopotential height variations in the tropics, while of weaker amplitude, exhibit far more zonal coherence.

The zonal coherence—or “dynamical annularity”, to use the terminology of Gerber & Thompson (2017)—of geopotential height variability is quantified in Figure 1a. Here and throughout the study, data is daily and is taken from ERA–Interim reanalysis (Dee et al., 2011) from 1 January 1979 to 31 December 2017, with eddy statistics provided by Martineau et al. (2018). JRA–55 (Kobayashi et al., 2015) reanalysis yields nearly identical results (not shown).



63 **Figure 1.** (a) The fraction of total variance associated with zonal mean anomalies in geopotential height (shaded), i.e., the power associated with wavenumber 0 in a zonal Fourier decomposition, normalized by the total power; and the RMS amplitude of the zonal mean flow (in  
 64 meters; contoured). Here and throughout the text, unless specified otherwise, anomalies are defined as departures from a seasonally evolving climatology and highpass-filtered with a 1 year  
 65 cutoff. (b) Correlation of 300 hPa geopotential height anomalies with our annular variability index  $\bar{Z}(300 \text{ hPa})$ , described in the text. Hatching indicates regions where the correlation is not  
 66 significantly different from 0 with 95% confidence, assuming a decorrelation time of 40 days to determine the degrees of freedom. (c) As in (b), but for the correlation of 850 hPa geopotential  
 67 height anomalies with the  $\bar{Z}(850 \text{ hPa})$  index.  
 68  
 69  
 70  
 71  
 72

73 In the midlatitude troposphere—from  $30^\circ$  to  $60^\circ$  latitude in both hemispheres—less  
 74 than 10% of variability is characterized by annular fluctuations. Near the poles, the  
 75 geometry of the sphere naturally leads to a dominance of zonally coherent motion, but an  
 76 additional maximum is observed in the tropics. Zonally coherent fluctuations of  
 77 geopotential height characterize thus approximately a quarter of tropical variability at  
 78 lower levels, the fraction increasing to almost a half at the tropopause. In this study, we  
 79 investigate the structure of this zonal mean, or annular, variability in the tropical  
 80 troposphere.

## 2 An index of zonal mean variability in the tropics

We first establish a convenient index to quantify annular variability in the tropics: zonal-mean geopotential height at the equator, computed on a given pressure level and denoted  $\bar{Z}(p)$ . We find that this simple index correlates very highly with more complex metrics, such as the leading time series from Principal Component Analysis of tropical geopotential height (cf. Baldwin & Thompson, 2009). Since these more complex options involve selecting parameters, we proceed with the simplest option. The data is filtered by subtracting the seasonal cycle and subsequently highpass-filtered with a 1-year cutoff to remove trends and low-frequency variability such as El Niño–Southern Oscillation (ENSO). As we discuss below, filtering is not critical.

Figure 1b,c shows the structure of variability associated with  $\bar{Z}(850)$  and  $\bar{Z}(300)$ . The indices characterize broad variations across the entire tropics, extending approximately  $20^\circ$  from the equator, particularly in the Pacific sector which dominates the zonal mean. Broad correlation in geopotential reflects the weak rotation in the tropical atmosphere. In the weak temperature gradient limit (Sobel et al., 2001), any localized heating or cooling of the atmosphere (e.g., by convection) is balanced by ascent or descent, thereby homogenizing the temperature, and hence geopotential height. The enhanced positive correlation in Figure 1b relative to Figure 1c reflects the increase in annular variability with height shown in Figure 1a.

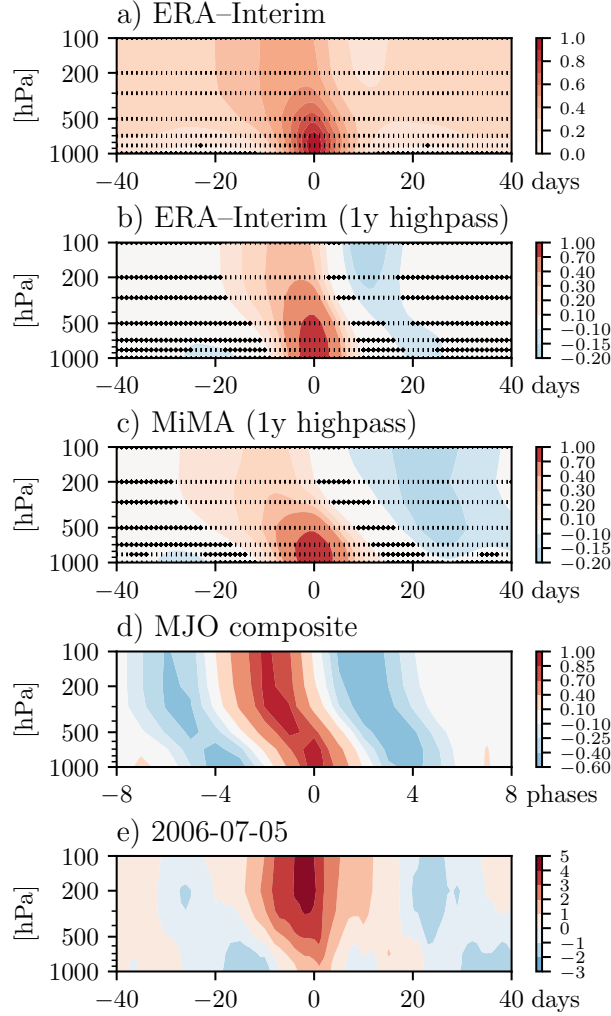
To characterize the zonal structure of variability, Gerber & Thompson (2017) suggest comparing single-point correlation maps in longitude, as shown in Figure S1. At lower levels, a given point is, on average, positively correlated with all other points around the latitude circle, the correlation decaying to zero towards the antipode. At upper levels, however, all points exhibit substantial positive correlation with others around the entire globe; at 300 hPa, the correlation is still approximately 0.4 at the antipode. This suggests that the zonal mean index characterizes broad variability at lower levels, albeit dominated by particular sectors at any given instant, which becomes increasing globally in nature in the upper troposphere. As a result, the zonal-mean index provides a convenient measure of large-scale variability across the tropics (Figure 1b,c), and capturing a substantial fraction of the total variability at all locations (Figure 1a).

## 3 Downward migration of annular circulation anomalies in the tropics

To explore the vertical coupling between zonal mean anomalies in geopotential height, Figure 2a shows the cross-correlation of  $\bar{Z}(p)$  with  $\bar{Z}(850)$ . We begin with unfiltered data (from which only the annual cycle has been removed), but even in this raw reanalysis data, we see a downward migration of geopotential height anomalies from the upper troposphere to the surface on a time scale of about 10 days, followed by the hint of an opposite-signed anomaly which also migrates downward. A comparable picture emerges if we choose other levels (e.g., 300 hPa) as our base level of correlation.

Low-frequency variability (primarily ENSO) and trends lead to significant redness in the unfiltered cross-correlations. The subseasonal time scale becomes more apparent after applying a highpass filtering with 1 year cutoff (Figure 2b). This conservative approach to removing the red background of the unfiltered cross-correlations still allows in more than half of the variance at a time scale of 1 year, and reveals more clearly a downward-migrating signal, anticorrelated with preceding and proceeding anomalies. In testing we find that the results are not sensitive to the cutoff provided it is short enough to remove ENSO.

Several approaches to significance testing underscore the robustness of this phenomenon. Hatching in Figure 2 indicates statistical significance assuming a decorrelation time scale of 40 days, a conservative approach to estimating the effective degrees of freedom. Subsetting the dataset by decades leads to similar results, as does



119 **Figure 2.** (a–d) Cross-correlation of  $\bar{Z}(p)$  with  $\bar{Z}(850)$ . Data (a) from ERA–Interim unfil-  
 120 tered, (b) from ERA–Interim with a 1-year highpass filter, (c) from MiMA with a 1-year highpass  
 121 filter, (d) composited by MJO RMM phase (amplitude-weighted; see text for details). (e) ERA–  
 122 Interim  $\bar{Z}(p)$  with a 1-year highpass filter, normalized to have unit variance, centered around July  
 123 5, 2006. In (a–c), hatching indicates inability to reject the null hypothesis that the correlation is  
 124 zero with 95% confidence, using a decorrelation time of 40 days.

137 employing composites instead of cross-correlations (not shown). Significance will further  
 138 be assessed dynamically and by comparing observations with a numerical model.

139 We first ask: is this downward migration simply the zonal mean manifestation of a  
 140 known tropical mode of variability? Both the MJO (Andersen & Kuang, 2012) and ENSO  
 141 (Seager et al., 2003) are known to exhibit zonally coherent variability. With respect to the  
 142 latter, the high pass filtering in Figure 2b is one approach to removing the ENSO signal.  
 143 (Alternatively, removing ENSO variability by regressing out the signal linearly correlated  
 144 with the Niño 3.4 index yields a very similar result to Figure 2a). The highpass filter,  
 145 however, will tend to amplify the relative importance of the MJO. To ensure the  
 146 downward migration exists independently of the MJO, we repeated the analysis after  
 147 regressing away variability linearly correlated with the principal components of the

148 Real-time Multivariate MJO (RMM) index (Wheeler & Hendon, 2004). Again, the results  
149 (not shown) are qualitatively identical with all MJO variability removed linearly.

150 As an additional approach to answering this question, we consider a numerical  
151 model which explicitly lacks ENSO or MJO-related variability. The Model of an Idealized  
152 Moist Atmosphere (MiMA; Jucker & Gerber, 2017) is an idealized aquaplanet, and  
153 modifications to the original model have been made to incorporate realistic zonal  
154 asymmetries in the lower boundary; a later iteration of this configuration has been  
155 published in Garfinkel et al. (2020). There is explicitly no oceanic variability and the  
156 model does not capture the MJO. The model has no cloud feedbacks and only resolves the  
157 large-scale circulation, employing a simplified parameterization of tropical convection.

158 Despite these substantial simplifications, geopotential anomalies also migrate  
159 downward in MiMA, on comparable temporal and vertical scales (Figure 2c). If anything,  
160 the cross-correlations in MiMA are slightly reduced in magnitude, implying that the full  
161 physics of the actual atmosphere act to strengthen the downward migration, rather than  
162 weaken it. Furthermore, the horizontal structure of tropical geopotential height variations  
163 in the model is comparable to Figure 1b,c (not shown).

164 We have shown idealized moist aquaplanet integrations because this is perhaps the  
165 simplest configuration that can reproduce the phenomenon. When one removes the  
166 impact of moisture from the model, as in the idealized atmospheric model of Held &  
167 Suarez (1994), the downward migration of geopotential anomalies is not apparent (not  
168 shown). Dry dynamical cores are fully capable of capturing the annular modes (e.g.,  
169 Gerber & Vallis, 2007), or the more recently discovered Baroclinic Annular Modes (Barnes  
170 & Thompson, 2014), but our results indicate that additional complexity is critical to  
171 capturing the annular variations of the tropics.

172 Although the MJO is not necessary for the downward-migrating signal in equatorial  
173 geopotential height, it does exhibit a similar signal. To quantify the MJO's signature on  
174 zonal-mean geopotential, we construct weighted composites of normalized geopotential  
175 anomalies at each level as a function of RMM phase (Wheeler & Hendon, 2004). Noting  
176 that 8 phases of the oscillation correspond to approximately 40 days, these composites  
177 show qualitatively similar downward migration on consistent time scales (Figure 2d).  
178 While a pure traveling wave would not project on to the zonal mean, we interpret this  
179 signal to be associated with the growth and decay of MJO anomalies. Thus in isolation an  
180 MJO event is sufficient, but not necessary, to achieve downward migration.

181 Besides the MJO, might other tropical waves play a role in the zonal mean?  
182 Convectively coupled tropical waves are a source of variability that is absent in a dry  
183 dynamical core, but present in the real atmosphere and MiMA. This is a difficult  
184 hypothesis to probe quantitatively, as filtering of tropical waves is typically nonlinear due  
185 to pre-filtering of the red background (e.g., Wheeler & Kiladis, 1999). We have shown  
186 that subseasonal anomalies emerge from a red spectrum (Figure 2a,b).

187 There is some theoretical evidence that zonally symmetric variability could also  
188 drive vacillations. Zhao & Ghil (1991) investigated symmetric inertial instability in a  
189 zonally averaged two-layer model and found a solution with zonal mean oscillations in  
190 geopotential shear. However, further investigation is needed to bridge their idealized  
191 study with observational data. In particular, our analysis indicates that eddy momentum  
192 fluxes also fluctuate coherently (Section 4), which suggests a pathway for waves to impact  
193 the zonal mean.

194 To get a sense of the actual variability, an example of downward migration for both  
195 positive and negative anomalies in the reanalysis record is shown in Figure 2e. The  
196 vertical coherence and time scales of these events are similar to the mean cross-correlated  
197 picture.

198 These events and the cross-correlated average are reminiscent of the “dripping paint  
 199 plots” of extratropical annular mode composites (Baldwin & Dunkerton, 2001), although  
 200 the resemblance is superficial, as the dynamics of the two are quite distinct. Downward  
 201 migration in the Northern and Southern annular mode indices involves coupling between  
 202 the tropospheric extratropical jet and the stratospheric polar vortex: a deceleration of the  
 203 polar vortex is usually followed by a nearly barotropic response in the troposphere  
 204 (Thompson & Wallace, 2000; Baldwin & Dunkerton, 2001). In the tropics, the downward  
 205 migration is entirely within the troposphere. In addition, downward migration in the  
 206 extratropical annular modes, while very robust, only appears in composite analysis and is  
 207 not evident from simple cross-correlation, unlike the tropical variability explored here.

208 Longitude–height cross-sections of geopotential height at key lags are shown in  
 209 Figure S2 (left column) to characterize the zonal structure of the downward migration.  
 210 Fluctuations of the zonal mean are positively correlated with individual points at all  
 211 longitudes, but an additional wave-1 structure indicates enhanced activity over the  
 212 Indo–Pacific as observed in Figure 1b,c. Similar coherence of geopotential height in  
 213 longitude and height are also observed with the 2006-07-05 event (Figure S2, right  
 214 column), albeit with additional variability on synoptic scales.

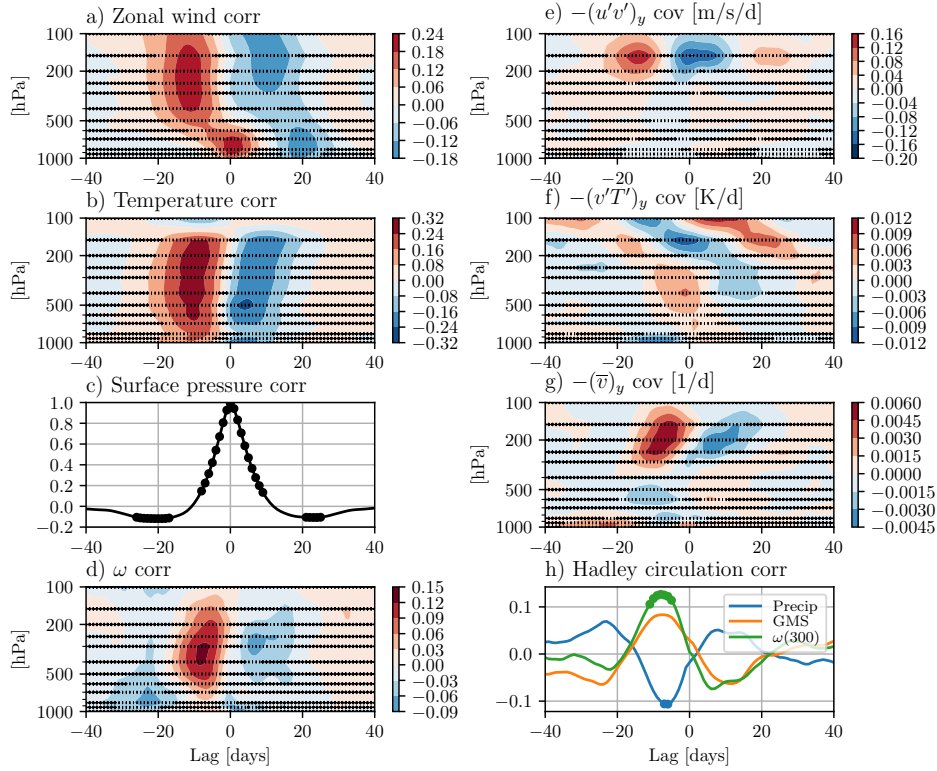
215 Downward migration in the tropical circulation is also apparent in other  
 216 meteorological variables, as shown in cross correlation of the zonal mean zonal wind with  
 217  $\bar{Z}(850)$  in Figure 3a. Weakened trade winds migrate downward in association with  
 218 anomalously high geopotential height, reflecting cyclostrophic balance. Conversely,  
 219 strengthened trade wind anomalies migrate downward in concert with negative  
 220 geopotential height anomalies. In the next section, we parse the structure of downward  
 221 migrating geopotential and zonal wind by cross-correlating with the key dynamical fields  
 222 at play.

#### 223 4 Mechanically forced variations in the Hadley Circulation

224 Geopotential height is the altitude of a given pressure surface of the atmosphere,  
 225 and thus depends on both the surface pressure and the temperature of the atmosphere  
 226 below. A pressure surface is elevated when the surface pressure increases; that is, when  
 227 the local mass of the atmospheric column is increased, requiring one to ascend higher  
 228 through the atmosphere to reach a given pressure. Similarly, a pressure surface is elevated  
 229 if the atmosphere below it is warmer, and so less dense, again requiring a higher ascent to  
 230 reach a given pressure. The downward migration of geopotential height anomalies shown  
 231 in Figure 2 thus corresponds to a coordination, or phase locking, between temperature  
 232 anomalies and surface pressure anomalies in the tropics.

245 Figure 3b,c show that anomalously high low-level geopotential (or surface pressure)  
 246 is preceded by anomalously warm temperatures throughout the tropical troposphere,  
 247 which lifts geopotential height at upper levels. Correlation between low-level geopotential  
 248 and temperature reaches a maximum at a lead of 10 days ( $-10$  on the horizontal axis), at  
 249 which time surface pressure anomalies are uncorrelated: the atmosphere is warmest when  
 250 surface pressure is neutral. The atmosphere cools as surface pressure anomalies build,  
 251 with temperature anomalies vanishing at lag 0, just as surface pressure reaches a  
 252 maximum. The atmosphere continues to cool, as surface pressure relaxes, reaching a  
 253 maximum negative anomaly near a lag of 10 days ( $10$  on the horizontal axis), maintaining  
 254 quadrature with the surface pressure field.

255 Since the surface pressure indicates the total mass of the atmospheric column,  
 256 downward migration in tropical geopotential can thus be described as a progression from  
 257 *hot to heavy* (more mass) to *cold*. The cross-correlation is symmetric, by construction, but  
 258 additional testing via composite analysis (not shown) reveals that this symmetry does



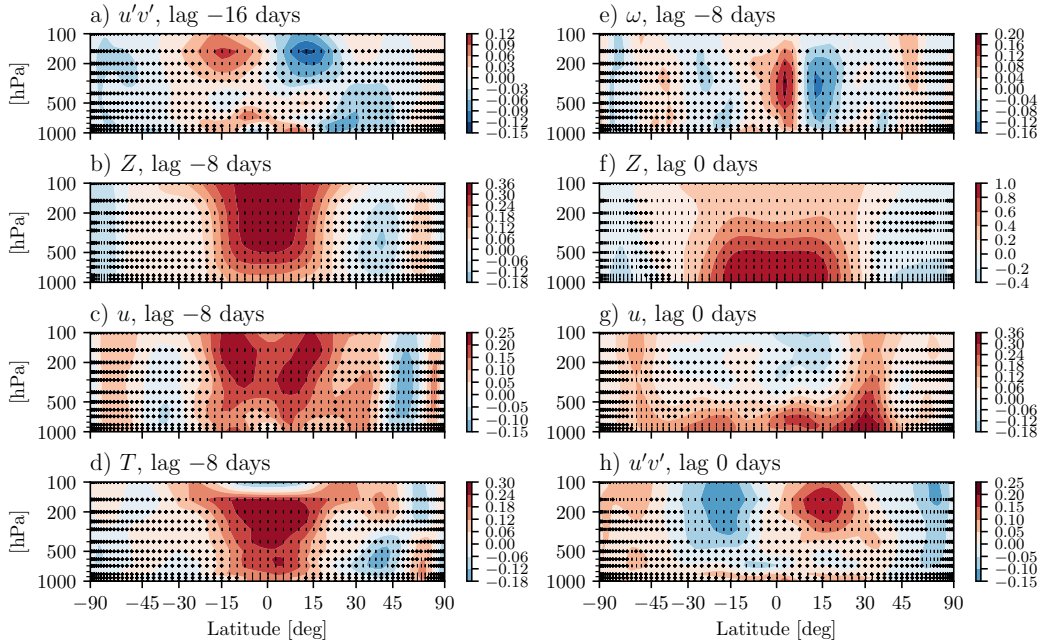
233 **Figure 3.** Cross-correlation and covariance of normalized  $\bar{Z}(850)$  with anomalous zonally averaged equatorial (a) temperature, (b) zonal wind, (c) surface pressure  $p_s$ , (d) pressure velocity  
 234  $\omega$ , (e) eddy momentum flux convergence, (f) eddy temperature flux convergence, (g) meridional  
 235 wind convergence, and (h) Hadley circulation metrics. Panels (a–d) and (h) are correlations;  
 236 panels (e–g) are shown as the covariance to give the dynamical tendencies physical units which  
 237 can be compared across pressure levels. In (h), the Hadley circulation is characterized by precipi-  
 238 tation rate (Precip), gross moist stability (GMS; moist static energy at 850 hPa minus 200 hPa),  
 239 and vertical velocity  $\omega$  at 300 hPa. Hatching and missing dots indicate the inability to reject the  
 240 null hypothesis at 95% confidence. We have assumed a conservative decorrelation time scale of  
 241 40 days for the more persistent fields in (a–c) and (h), as in previous figures. The decorrelation  
 242 scale of eddy fluxes,  $\omega$ , and  $v_y$  is much shorter, on the order of days. For (d–g), we have therefore  
 243 assumed a time scale of 10 days.  
 244

259 hold between positive and negative anomalies: downward migration of negative  
 260 geopotential height anomalies are associated with a cold–light–warm pattern.

261 This phase locking between temperature and surface pressure reflects a common  
 262 dynamical origin: a pulsing of the Hadley circulation, seen in the vertical (pressure)  
 263 velocity in Figure 3d and other metrics in Figure 3h. The positive correlation between the  
 264 pressure velocity  $\omega$  and temperature, however, indicates that the anomalies must be  
 265 mechanically forced: warmer temperature is associated with anomalous downwelling. For  
 266 thermodynamic forcing to create kinetic energy, warm air must rise. This suggests that  
 267 the temperature tendency is more attributable to the anomalous downwelling, which  
 268 reduces the overall adiabatic cooling by the ascending branch of the Hadley Circulation.  
 269 We also observe a concomitant reduction in precipitation in Figure 3h, suggesting that the  
 270 temperature anomalies are not being forced by enhanced latent heating. The reduction in

271 precipitation is consistent with increase in gross moist stability associated with warming  
 272 of the free troposphere.

273 The dynamical origin of the vacillation can be traced back to anomalous eddy-driven  
 274 momentum convergence in the upper troposphere at a lead time of 16 to 20 days relative  
 275 to the  $\bar{Z}(850)$  index, as seen in Figure 3e. The eddy forcing can be characterized by the  
 276 divergence of the momentum flux at the equator, which reflects a broad anomaly in  
 277 momentum forcing across the tropics, as shown in the meridional cross-section of the  
 278 momentum flux at a lead of 16 days in Figure 4a. This positive anomaly reflects a  
 279 weakening of the climatological momentum flux out of the tropics, which drives the  
 280 downwelling anomaly peaking at a lead of 8 days (Figure 3d) as in the eddy-driven pump  
 281 mechanism of Holton et al. (1995). Strictly speaking, this mechanism cannot be applied at  
 282 the equator, but the momentum flux anomaly is spread over the tropics (Figure 4a).  
 283 Momentum fluxes out of the Hadley circulation allow flow across angular momentum  
 284 surfaces, enhancing the thermodynamically driven cell. A weakening of momentum flux  
 285 leads to a temporary slowdown of the circulation, particularly at upper levels, which can  
 286 be inferred from the convergence of the meridional velocity ( $-v_y$ ), shown in Figure 3g.



287 **Figure 4.** Cross-correlations of  $\bar{Z}(850)$  with zonal mean fields as a function of latitude (de-  
 288 grees) and height (hPa) at varying lead/lag times: (a) eddy momentum flux (lag  $-16$  days), (b)  
 289 geopotential height ( $-8$  days), (c) zonal wind ( $-8$  days), (d) temperature ( $-8$  days), (e) pressure  
 290 velocity ( $-8$  days), (f) geopotential height (0 days), (g) zonal mean wind (0 days), and (h)  
 291 eddy momentum flux (0 days). As before, fields are climatological anomalies and highpass-filtered  
 292 with a cutoff of 1 year. Negative lags indicate that the specified field leads  $\bar{Z}(850)$ . Statistical  
 293 significance is assessed as in Figure 3: 40 days for (b,c,d,f,g), and 10 days for (a,e,h).

294 At a lead time of 8 days, broad anomalies in geopotential and temperature  
 295 anomalies are observed throughout the tropics, extending  $20^\circ$  into each hemisphere, as  
 296 shown in the meridional cross-sections in Figure 4b,c. Anomalies in the trade winds peak  
 297 off the equator, near  $10^\circ\text{N}$  and S. The pressure velocity field at the same time, shown in  
 298 Figure 4e, exhibits more fine scale structure. A reduction of upwelling (positive  $\omega$ ) is

299 observed within  $10^\circ$  of the equator in both hemispheres, but the correlation is stronger in  
 300 the Northern Hemisphere. Anomalous upwelling is observed polewards of  $10^\circ$ , again, more  
 301 significantly in the boreal hemisphere. This suggests that a simple reduction in adiabatic  
 302 expansion driven by the reduction of upwelling cannot explain the meridional temperature  
 303 structure. A detailed budget is the subject of further analysis, but we find that the eddy  
 304 temperature flux (Figure 3f) generally acts to damp the temperature anomalies, although  
 305 it exhibits evidence of a signal extending higher into the stratosphere.

306 Figure 4f,g,h shows the correlation of anomalies of zonal mean geopotential height,  
 307 wind, and eddy momentum flux, concomitant with maximum positive anomalies of  
 308  $\bar{Z}(850)$ . As seen in Figure 2, geopotential height anomalies have descended toward the  
 309 surface across the tropics from  $20^\circ\text{S}$  to  $20^\circ\text{N}$ , peaking at levels below 500 hPa, and  
 310 associated with low level trade wind anomalies that extend further into the extratropics.  
 311 Eddy momentum flux anomalies have flipped sign relative to earlier lags, driving the  
 312 subsequent propagation of opposite anomalies in height and wind at positive lags,  
 313 essentially repeating the same cycle, but with opposite sign.

314 Lastly, it is important to account for the surface pressure anomalies, which are  
 315 essential to the downward propagating signal. The slowdown of the circulation before lag  
 316 0 also enhances mass convergence over the equator, focused at upper levels where the  
 317 tropospheric branch of the Hadley circulation diverges (Figure 3g). This accounts for the  
 318 surface pressure fluctuations, as the meridional contribution to the surface pressure  
 319 tendency is (in pressure coordinates):

$$320 \quad \frac{\partial \bar{p}_s}{\partial t} = -\frac{\partial}{\partial y} \overline{\int_0^{p_s} v \, dp} = -\int_0^{\bar{p}_s} \frac{\partial \bar{v}}{\partial y} \, dp - \overline{v(p_s) \frac{\partial p_s}{\partial y}} - \overline{\int_{\bar{p}_s}^{p_s} \frac{\partial v'}{\partial y} \, dp}. \quad (1)$$

321 The zonal average tendency is dominated by the vertical integral of  $-\bar{v}_y$  (the first term on  
 322 the RHS) as mass convergence is occurring at upper levels, rather than at the lower  
 323 boundary (the second and third terms on the RHS). The convergence of mass is consistent  
 324 with the slowdown in the circulation driven by momentum fluxes, peaking in the upper  
 325 half of the atmosphere where the momentum forcing is strongest.

326 We acknowledge that cross-correlation analysis does not indicate causation, and that  
 327 the signals presented in Figures 3 and 4 are weak relative to background noise, i.e., the  
 328 abundance of tropical processes that survive the 1-year high pass filter. More aggressive  
 329 filtering increases the magnitude of the correlation (not shown), but we have taken a  
 330 conservative filtering approach to avoid artificially amplifying variability on subseasonal  
 331 timescales. Our confidence in the mechanism rests primarily on the dynamical consistency  
 332 between the eddy forcing and zonal mean circulation eddies, taken together. It is an open  
 333 question as to what drives the anomalous eddy forcing that triggers the cycle, and further  
 334 research is required to untangle the role of tropical and extratropical wave sources.

## 335 5 Summary

336 Annular variations in geopotential height capture a higher fraction of the natural  
 337 variability in the tropical atmosphere as compared to the midlatitudes. We constructed a  
 338 simple index to characterize the annular variability of the tropics: zonal-mean  
 339 geopotential at the equator. The index tracks broad variations of the height fields at each  
 340 level, extending approximately 20 degrees in latitude into both hemispheres.  
 341 Cross-correlation between levels reveals downward-migrating circulation anomalies on  
 342 intraseasonal time scales. Positive geopotential height anomalies, associated with  
 343 decreased trade winds, migrate from the tropopause to the surface on a time scale of  
 344 approximately 10 days. Likewise, enhanced trade winds migrate downward with negative  
 345 geopotential height anomalies.

346 While the Madden–Julian Oscillation (MJO) is associated with a similar zonal mean  
 347 signature, we find that these downward migration circulation anomalies are more generic.

They reflect a phase locking of temperature and surface pressure anomalies associated with variations in the overturning circulation on subseasonal time scales. Anticorrelation between the vertical velocity and temperature indicates that these variations are mechanically driven, consistent with anomalies in eddy momentum flux convergence. Simulations with idealized atmospheric models attest to the generic nature of these downward migrating anomalies, but indicate that the mechanism depends on the presence of tropical variability. Future work intends to explore the mechanism in greater detail, and investigate the predictability of these oscillations.

### Acknowledgments

We thank Olivier Pauluis, David Thompson, and an anonymous reviewer for helpful discussion and feedback on earlier versions of this manuscript. This research was supported by the NSF through grant AGS-1852727 to New York University. KD also acknowledges support from the NASA Postdoctoral Program at the Goddard Institute for Space Studies.

Data availability. This study is based on atmospheric reanalyses and integrations with an idealized model atmospheric model. ERA–Interim reanalysis was obtained from ECMWF at <https://apps.ecmwf.int/datasets/> and is documented by (Dee et al., 2011). Eddy statistics derived from ERA–Interim were provided by Martineau et al. (2018), available at <https://catalogue.ceda.ac.uk/>. Key results were checked with JRA-55 reanalysis (not shown), available and documented at [https://jra.kishou.go.jp/JRA-55/index\\_en.html](https://jra.kishou.go.jp/JRA-55/index_en.html). MiMA is documented by Jucker & Gerber (2017) and Garfinkel et al. (2020). The source code and run parameters for the original MiMA model are available at <https://github.com/mjucker/MiMA>, and the modified configuration at <https://doi.org/10.5281/zenodo.1401407>.

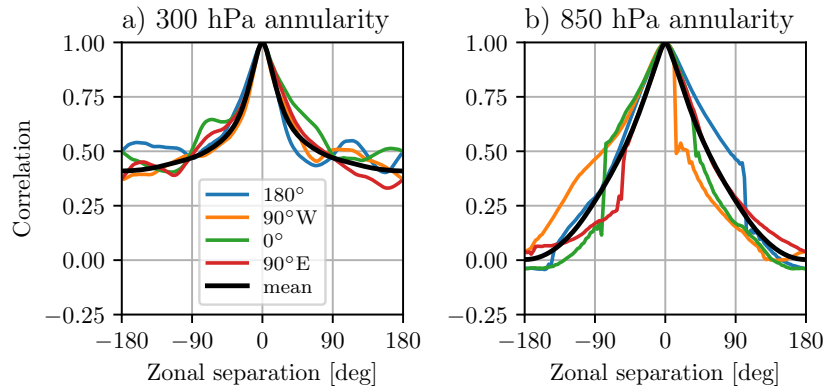
### References

- Ambaum, M. H., Hoskins, B. J., & Stephenson, D. B. (2001). Arctic Oscillation or North Atlantic Oscillation? *Journal of Climate*, *14*(16), 3495–3507.
- Andersen, J. A., & Kuang, Z. (2012). Moist static energy budget of MJO-like disturbances in the atmosphere of a zonally symmetric aquaplanet. *Journal of Climate*, *25*(8), 2782–2804.
- Baldwin, M. P., & Dunkerton, T. J. (2001). Stratospheric Harbingers of Anomalous Weather Regimes. *Science*, *294*(5542), 581–584.
- Baldwin, M. P., & Thompson, D. W. (2009). A critical comparison of stratosphere–troposphere coupling indices. *Quarterly Journal of the Royal Meteorological Society*, *135*(644), 1661–1672.
- Barnes, E. A., & Thompson, D. W. (2014). Comparing the roles of barotropic versus baroclinic feedbacks in the atmospheres response to mechanical forcing. *Journal of the Atmospheric Sciences*, *71*(1), 177–194.
- Dee, D. P., Uppala, S. M., Simmons, A. J., Berrisford, P., Poli, P., Kobayashi, S., . . . Geer, A. J. (2011). The ERA-Interim reanalysis: configuration and performance of the data assimilation system. *Q. J. R. Meteorol. Soc.*, *137*, 553–597.
- Deser, C., Walsh, J. E., & Timlin, M. S. (2000). Arctic sea ice variability in the context of recent atmospheric circulation trends. *Journal of Climate*, *13*(3), 617–633.
- Feldstein, S. B. (2000). The timescale, power spectra, and climate noise properties of teleconnection patterns. *Journal of Climate*, *13*(24), 4430–4440.
- Garfinkel, C. I., White, I., Gerber, E. P., Jucker, M., & Erez, M. (2020). The building blocks of northern hemisphere wintertime stationary waves. *Journal of Climate*(2020).
- Gerber, E. P., & Thompson, D. W. J. (2017). What Makes an Annular Mode Annular? *Journal of the Atmospheric Sciences*, *74*(2), 317–332.

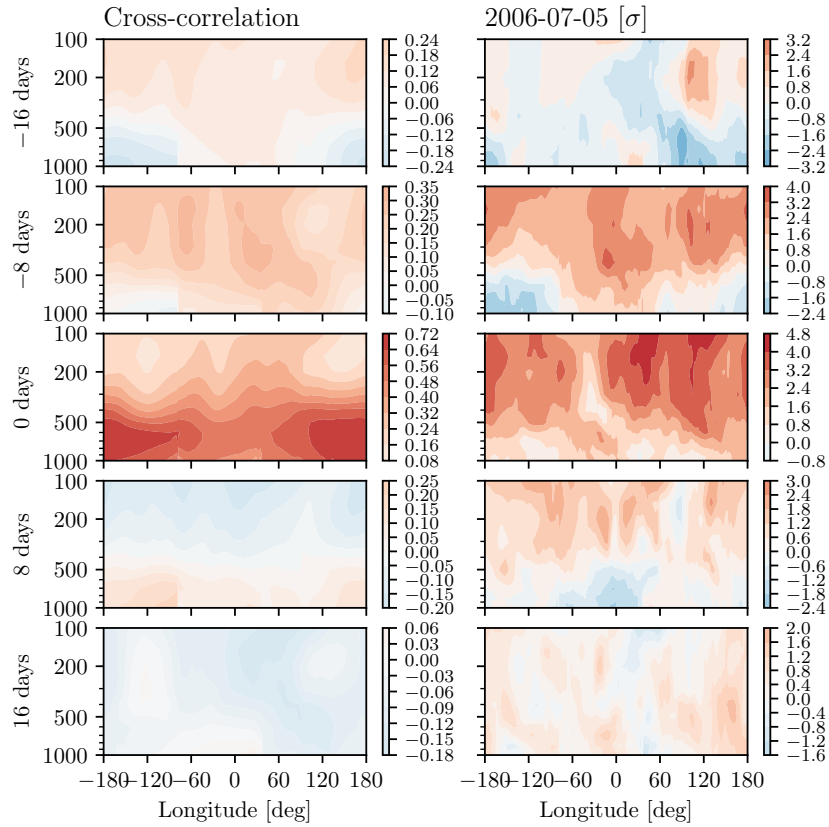
- 398 Gerber, E. P., & Vallis, G. K. (2007). EddyZonal Flow Interactions and the Persis-  
 399 tence of the Zonal Index. *J. Atmos. Sci.*, *64*(9), 3296–3311.
- 400 Hartmann, D. L., & Lo, F. (1998). Wave-driven zonal flow vacillation in the south-  
 401 ern hemisphere. *Journal of the Atmospheric Sciences*, *55*(8), 1303–1315.
- 402 Held, I. M., & Suarez, M. J. (1994). A Proposal for the Intercomparison of the  
 403 Dynamical Cores of Atmospheric General Circulation Models. *Bull. Am. Meteorol.*  
 404 *Soc.*, *75*(10), 1825–1830.
- 405 Holton, J. R., Haynes, P. H., McIntyre, M. E., Douglass, A. R., & Rood, B. (1995).  
 406 Stratosphere-Troposphere Exchange. *Rev. Geophys.*, *33*(4), 403–439.
- 407 Jucker, M., & Gerber, E. P. (2017). Untangling the annual cycle of the tropical  
 408 tropopause layer with an idealized moist model. *J. Clim.*, *30*(18), 7339–7358.
- 409 Kobayashi, S., Ota, Y., Harada, Y., Ebata, A., Moriya, M., Onoda, H., . . . Kiy-  
 410 otoshi, T. (2015). The JRA-55 reanalysis: General specifications and basic  
 411 characteristics. *Journal of the Meteorological Society of Japan*, *93*(1), 5–48.
- 412 Kushner, P. J. (2010). Annular modes of the troposphere and stratosphere. *Geo-*  
 413 *physical Monograph Series*, *190*(1), 59–91.
- 414 Martineau, P., Wright, J. S., Zhu, N., & Fujiwara, M. (2018). Zonal-mean data set  
 415 of global atmospheric reanalyses on pressure levels. *Earth System Science Data*,  
 416 *10*(4), 1925–1941.
- 417 Seager, R., Harnik, N., Kushnir, Y., Robinson, W., & Miller, J. (2003). Mechanisms  
 418 of hemispherically symmetric climate variability. *Journal of Climate*, *16*(18),  
 419 2960–2978.
- 420 Sobel, A. H., Nilsson, J., & Polvani, L. M. (2001). The Weak Temperature Gradient  
 421 Approximation and Balanced Tropical Moisture Waves. *Journal of the Atmo-*  
 422 *spheric Sciences*, *58*(23), 3650–3665.
- 423 Thompson, D. W. J., Solomon, S., & Hill, L. (2002). Interpretation of Recent South-  
 424 ern Hemisphere Climate Change. *Science*, *296*(5569), 895–899.
- 425 Thompson, D. W. J., & Wallace, J. M. (1998). The arctic oscillation signature in the  
 426 wintertime geopotential height and temperature fields. *Geophysical research let-*  
 427 *ters*, *25*(9), 1297–1300.
- 428 Thompson, D. W. J., & Wallace, J. M. (2000). Annular Mode in the Extratropical  
 429 Circulation. Part I : Month-to-Month Variability. *J. Clim.*, *13*(1999), 1000–1016.
- 430 Thompson, D. W. J., Wallace, J. M., & Hegerl, G. C. (2000). Annular modes in the  
 431 extratropical circulation. part ii: Trends. *Journal of climate*, *13*(5), 1018–1036.
- 432 Wheeler, M., & Hendon, H. H. (2004). An all-season real-time multivariate mjo in-  
 433 dex: Development of an index for monitoring and prediction. *Monthly weather re-*  
 434 *view*, *132*(8), 1917–1932.
- 435 Wheeler, M., & Kiladis, G. N. (1999). Convectively coupled equatorial waves: Anal-  
 436 ysis of clouds and temperature in the wavenumber–frequency domain. *Journal of*  
 437 *the Atmospheric Sciences*, *56*(3), 374–399.
- 438 Zhao, J. X., & Ghil, M. (1991). Nonlinear Symmetric Instability and Intraseasonal  
 439 Oscillations in the Tropical Atmosphere. *Journal of the Atmospheric Sciences*,  
 440 *48*(24), 2552–2568.

441

## Supplemental figures



442 **Figure S1.** Pairwise correlation between geopotential height anomalies on the equa-  
 443 tor as a function of longitudinal separation at (a) 300 and (b) 850 hPa. Explicitly, this is:  
 444  $\text{corr}(Z_{\lambda_0}, Z_{\lambda_0 + \Delta\lambda})$ , for four base longitudes  $\lambda_0$  (indicated by the legend) as a function of zonal  
 445 separation  $\Delta\lambda$  in degrees longitude. As explored by Gerber & Thompson (2017), this allows one  
 446 to compare the correlation structure in different sectors. The black line is the mean of the corre-  
 447 lation maps over all longitudes (not just the four points shown). As with the analysis in the main  
 448 text, anomalies are climatological and highpass-filtered with a cutoff of 1 year. The abrupt drops  
 449 and kinks in correlation at 850 hPa are associated with orography at the equator.



450 **Figure S2.** (a) Cross-correlation of equatorial geopotential anomalies with  $\bar{Z}(850)$  at specified  
 451 lead/lag times as a function of longitude (degrees) and height (hPa). (b) Snapshots of the corre-  
 452 sponding profiles for the 2006-07-05 event, at the same lags (e.g., the top panel shows anomalies  
 453 on 2006-06-19, 16 days before the central event date). Anomalies have been normalized to have  
 454 unit variance at all longitudes and pressure levels, so that the units are standard deviations  $\sigma$ .